PCCP

Accepted Manuscript

ROYAL SOCIETY OF CHEMISTRY

www.rsc.org/pccp

PCCP

ARTICLE

A comparative first principle study on trivalent ions incorporated SSZ-13 zeolites

Received 00th January 20xx,

Accepted 00th January 20xx

DOI: 10.1039/x0xx00000x

www.rsc.org/

Cui Wen,[a] Lu Geng,[a] Lina Han,[a] Jiancheng Wang,[b]* Liping Chang,[b] Gang Feng,[c,d] Dejin Kong,[d] and Jianwen Liu [e]*

The dispersion-corrected density functional theory has been used to study the trivalent ions B, Al, Ga, and Fe incorporated SSZ-13-type zeolites. The associated structure and Brønsted/Lewis acidity change caused by the incorporation ions were comparatively studied. It was found that the smaller radius differences of the incorporation ions are, the smaller changes of structure will be and the less acidity will be enhanced for the Brønsted sites. The trivalent Al is found the most favorable trivalent incorporation ion and Na is found the most favorable charge balanced ion for the synthesis of SSZ-13-type zeolites due to size comparability, which are in line with the experimental observation. The substitution energies which show the relative synthesis difficulty level were also applied for B, Al, Ga, and Fe incorporated zeolites and found the difficulty decreases with order of Fe > B > Ga >> Al, also in good agreement with the experimental observations. Adsorption studies for the NH_3 and pyridine molecules indicate that adsorption on the Brønsted acid sites are more stable than on the Lewis acid sites. The Brønsted acidity were found to follow the order of HAl-SSZ-13 > HGa-SSZ-13 ≈ HFe-SSZ-13 > HB-SSZ-13 where the Lewis acidity was found to follow the order of HGa-SSZ-13 ≈ HFe-SSZ-13 > HAl-SSZ-13 > HB-SSZ-13. Our results provide new insights for the synthesis of the SSZ-13-type zeolites and fundamental information for the zeolitic catalyst designation to enhance the catalytic performance.

1. Introduction

Zeolites with well-defined channel systems and cavities [1, 2] have been widely used as catalysts, adsorbents and ion-exchangers in industry [3, 4] due to their outstanding solid-acidicity, adsorption-desorption properties and shape-selectivity. The SSZ-13 zeolite (CHA-type), which is in the monoclinic space group R/3m with the lattice parameters of a = b = 13.675 Å, c = 14.767 Å, α = β = 90.0°, γ = 120.0° and each unit cell contains $Si_{36}O_{72}$, were discovered by Zones and coworkers.[5, 6] Its framework is decorated by a 3-dimensional interconnected pore system with 8-membered ring windows (3.8 Å×3.8 Å) and a relatively low framework density (15.1 T/1000 $Å^3$).[7, 8] Previously, many works investigated the preparation methods,[5, 9, 10] the acid properties,[11, 12] and the catalytic performance.[13-15] SSZ-13, especially for Al incorporated SSZ-13 is typically synthesized in the Na form and some other ions can be exchanged afterwards to form the other form SSZ-13 zeolites such as H-SSZ-13, Li-SSZ-13, K-SSZ-13 and NH_4-SSZ-13.[5, 16] Because of its unique pore configuration as well as acid properties, SSZ-13 has been widely used for the separation of CO_2 [17, 18] and methanol-to-olefin (MTO) conversion reaction.[13, 19] Due to its high activity, SSZ-13 can also be used as the catalyst for the selective catalytic reduction (SCR) of NOx in the presence of NH_3, which make it one of the most studied zeolites today. [20-22] Previoulsy Goeltl and coworkers have identified the complex IR spectrum of NO adsorption on divalent copper sites of copper-exchanged SSZ-13 with detailed electronic structures,[21, 22] which facilitates the tailor-made catalyst for SCR of NOx for the commercial application.

To modify the properties of the zeolitic internal wall for its application, trivalent ions such as Al, B, Ga and Fe [9, 19, 23-25] are usually used to replace the silicons inside the zeolites employing a monovalent atom or group such as H^+, Li^+, Na^+, K^+ and NH_4^+ to balance the additional charges.[26, 27] As the valences of these ions are different from that of silicons, the Brønsted and Lewis acid properties are hereby introduced, which influence the acid properties and the performance of the catalyst.[28, 29] Previsouly, the acidicity characterization, structure prediction and adsorption have been extensively studied for various zeolites with incorporated ions.[30-33]

Among these trivalent incorporation ions, Al is the mostly used one as it has the smallest radius difference from the silicon experimentally. The incorporation of Al can create acid

[a] College of Materials Science and Engineering, Taiyuan University of Technology, Taiyuan 030024, P.R. China.
[b] Key Laboratory of Coal Science and Technology, Ministry of Education and Shanxi Province, Taiyuan University of Technology, Taiyuan 030024, P. R. China.
[c] College of Chemistry, Nanchang University, Nanchang, Jiangxi 330031, P.R. China
[d] Shanghai Research Institute of Petrochemical Technology SINOPEC, Shanghai, 201208, P.R. China
[e] National Supercomputing Center in Shenzhen, Shenzhen, 518055, P.R. China
† E-mail: wangjiancheng@tyut.edu.cn (J.C. W.) and liujw@nsccsz.gov.cn (J.W. L.)
Electronic Supplementary Information (ESI) available: [details of any supplementary information available should be included here]. See DOI: 10.1039/x0xx00000x

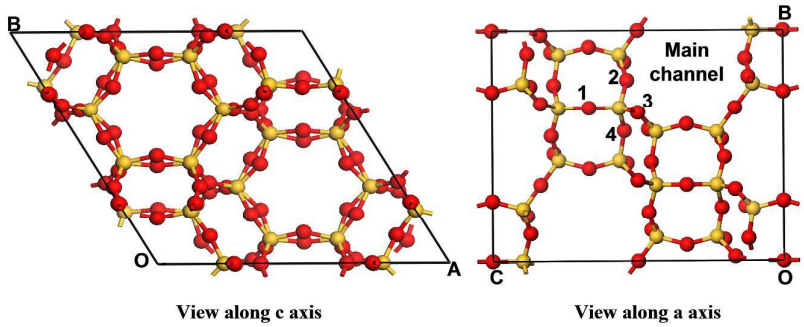

Fig. 1. The cell of SSZ-13-type zeolite. The Si and O atoms are shown in yellow and red, respectively. Four different bridges O are marked by number 1-4.

sites with less structural deformation. The distribution of Al in SSZ-13 and other CHA zeolites were extensively studied previously not only experimentally but also theoretically.[34-37] Jeanvoine and coworkers studied the substitution effects of Al for CHA using periodic models, in which the calculated OH stretching frequencies of acidic protons were in agreement with experimental infrared spectra of H-SSZ-13.[35] de Vries and coworkers studied the D/H-exchange barriers for methane at the isolated Brønsted sites in CHA using combined quantum-chemical-classical (QM/MM) calculations and found that energy barrier depends on geometric structure for the transition state accommodation.[36] Zokaie and coworkers studied the Al distribution in CHA zeolites and found that the more stable of the acid sites, the weaker strength of the Brønsted acid.[23]

For the B incorporated CHA zeolites, It was also found by ^{11}B MAS NMR that all the boron atoms are incorporated into the framework as tetrahedral BO_4 units in the as-synthesized samples and the thermal stability of the B-SSZ-13 borosilicate decreased as the boron content increases. [38] The Si/B ratios were found in the range of 11.8 to 6.9. The B-K-edge XANES and DFT [39, 40] were applied to study the isomorphous substitution of B^{3+} into the CHA framework (B-SSZ-13) before and after template removal, which showed that the prepared B-SSZ-13 exhibits $[B(OSi)_4]$ units while, upon template burning, the break of a B-O-Si bond results in $[B(OSi)_3]$ units. For the Ga-SSZ-13 zeolites, the ^{71}Ga NMR characterizations showed that the Ga is incorporated into the framework of these zeolites and the infrared bands at 3600 cm^{-1} was observed for Ga-SSZ-13 zeolites, which showed the weak Brønsted acidity.[19] For Ga incorporated SSZ-13, Fricke *et al.* [41] reviewed the properties and found that the Ga-incorporated zeolites show weaker acidity than Al incorporated zeolites, while it is stronger than those of Fe- or B-incorporated zeolites. Moreover, it is found that with an increase of the Ga content incorporated into the SAPO-34 framework the acid sites and particle size decreased, which also caused the collapses of framework of SAPO-34.[42] For the Fe incorporated SSZ-13 zeolites, the EPR data showed that tetrahedral Fe^{3+} coordination in the lattice was observed and different octahedral signals in the impregnated Fe-CHA materials were found.[43]

Previous studies on B, Al, Ga, and Fe incorporated SSZ-13 zeolites have demonstrated that the incorporations of different trivalent ions and monovalent atoms indeed affect the acidity, catalysis performance and the adsorption-desorption properties. It is also found that the acidity of zeolites plays an essential role in the transformation of methanol to olefin and the shape selectivity reactions. For Al-SSZ-13 zeolites and Ga-SSZ-13, methanol can be efficiently activated on the Brønsted acid,[13, 19] which shows promising potential for MTO commential application. The B-SSZ-13 zeolites can be applied to the reaction of the methanol to hydrocarbon conversion due to shape-selectivity.[44] For Fe-SSZ-13 zeolites, α-oxygen can be formed on di-nuclear iron sites which can be used as the catalyst for N_2O decomposition and methane partial oxidation at elevated temperatures.[43]

However, the incorporation effect which leads to the associated structures change as well as the Brønsted and Lewis acid properties are still unknown at the molecular level although the Al incorporated SSZ-13 zeolites have somehow been discovered. To better understand these properties at molecular level, the B, Al, Ga and Fe incorporation effect and associated property modification were comparatively studied for SSZ-13 type zeolites using dispersion corrected periodic density functional theory in present work.

2. Calculation Details

The dispersion-corrected periodic density functional method as implemented in the Vienna *ab* initio Simulation Package (VASP) was used for all the calculations.[45, 46] The DFT-D2 method of Grimme was used to take into account the dispersive interactions[47, 48] as previously we found the dispersion correction is important for the MTW-type zeolites[25], $AlPO_4$-5 zeolites[49] and vanadium oxide.[50] The exchange and correlation energies were calculated by the generalized gradient approximation (GGA) formulation with the PBE functional.[51] The Kohn-Sham one-electron states were extended in accordance with plane-wave basis sets with a kinetic energy of 400 eV. The projector augmented wave (PAW) method was applied to describe the electron-ion interactions.[52, 53] The DFT+U calculations were performed for

the strong on-site Coulomb repulsion for the *d* electrons with the U – J = 4.3 eV for Fe atoms following previous works.[54, 55] The Brillouin zone was sampled with a 3×3×3 *k*-points mesh, generated by the Monkhorst-Pack algorithm, for the SSZ-13-type unit cell. The convergence criteria were set 1.0×10^{-4} eV for the SCF energy, 1×10^{-3} eV and 0.05 eV/Å for the total energy and the atomic forces, respectively. For structure optimizations, the atoms and the cell parameters of SSZ-13 lattice were fully relaxed.

As shown in Fig. 1, each unit cell ($Si_{36}O_{72}$) of the SSZ-13-type structure is composed of double six-rings, which are connected with 4 member ring (4MR), and its main channel is 8MR. All the tetrahedral (T) sites of SSZ-13 framework are equivalent while there are four kinds of inequivalent oxygen sites.[11] To investigate the low-lying structures and acid properties of the zeolites, one Si atom was substituted by one trivalent atom M (M = B, Al, Ga, Fe) in the unit cell to get the Si/M ratio at 35. In order to maintain the charge balance of the zeolites, we used the monovalent ions and group (H^+, NH_4^+, Li^+, Na^+ and K^+) to balance the charge. In order to locate the low-lying structures for the monovalent ions bonds to each oxygen atom, we calculated the monovalent atoms pointing to different nearby O atoms. The optimized structures of the H-form SSZ-13 were used to investigate the adsorption of NH_3 and pyridine. Both the Lewis and Brønsted acid sites were considered for the adsorption of NH_3 and pyridine in both the main channel (8MR) and the cage of the zeolite.

In order to study the influences of the substituted trivalent M (M = B, Al, Ga, Fe) and charge balanced ions/groups Y (Y = H^+, Li^+, Na^+, K^+) to the thermochemistry of the zeolites synthesis reactions, we calculated the reaction of 36 $Si(OH)_4$ molecules to produce a *p*(1×1×1) SSZ-13-type zeolites cell ($Si_{36}O_{72}$) and 72 H_2O molecules. It shows that the pure silica SSZ-13 zeolites synthesis reaction releases –29 kJ • mol^{-1}, which indicates an exothermic reaction similar to that for the pure silica MTW zeolites.[25] The incorporation of one M atom into the SSZ-13 framework could be considered as the substitution of one Si atom of the pure silica zeolites by one M and Y atoms, which described as the following reaction:

$$(\text{O-Si-O})_n^{\text{SSZ-13}} + n\text{M(OH)}_3 + n\text{YOH} \rightarrow n\text{Si(OH)}_4 + (\text{O-M-OY})_n^{\text{SSZ-13}} \quad \text{(a)}$$

where M = B, Al, Ga, Fe; Y = H, NH_4, Li, Na, K; *n* = 1, 2, 3, … The associated substitution energy could be calculated as following:

$$E_{sub} = nE[\text{Si(OH)}_4)] + E[(\text{O-M-OY})_n^{\text{SSZ-13}}] - E[(\text{O-Si-O})_n^{\text{SSZ-13}}] - nE[\text{M(OH)}_3] - nE[\text{YOH}] \quad \text{(b)}$$

Where $E[\text{Si(OH)}_4)]$, $E[(\text{O-M-OY})_n^{\text{SSZ-13}}]$, $E[(\text{O-Si-O})_n^{\text{SSZ-13}}]$, $E[\text{M(OH)}_3]$ and E[YOH] are the total energies of the free $Si(OH)_4$, YM-SSZ-13 zeolite cell, pure silica SSZ-13-type zeolite cell, free $M(OH)_3$ and YOH molecules, respectively. As described in our previous works,[9, 25] from the thermodynamical point of view, E_{sub} could be used to evaluate the prescriptions for zeolite synthesis. Take M-SSZ-13 as an example, for a given *n*, E_{sub} is a function of Y, a larger E_{sub} indicates a thermodynamically more preferred Y and M for the SSZ-13 zeolite synthesis. For a given Y and M, E_{sub} is a function of *n*, a larger E_{sub} indicates preferred Si/M ratio for the zeolite.

The adsorption energies (E_{ads}) for the adsorption of NH_3 and pyridine in the zeolite were calculated by

$$E_{ads} = E(\text{molecule@SSZ-13}) - [E(\text{molecule}) + E(\text{SSZ-13})] \quad \text{(c)}$$

Where E(molecule@SSZ-13), E(molecule) and E(SSZ-13) are the total energies of the SSZ-13-type zeolite cell with adsorbed molecule in the pore, the gas phase NH_3/pyridine molecules and the SSZ-13-type zeolite, respectively. The larger adsorption energy indicates the stronger adsorption for the probed molecules on the acid sites.

3. Results and discussions

3.1 Structures

The most stable structures searching were performed systematically for the B, Al, Ga and Fe incorporated SSZ-13-type zeolites, in which the H^+, Li^+, Na^+, and K^+ were used to balance the additional charge caused by the substitution. The associated most stable structures were shown in Fig. 2–5. And the relative energies for the B, Al, Ga and Fe incorporated SSZ-13-type zeolite were shown in Table S1. For the convenience of discussion, a nomenclature Y-M-*x*MR is used for the following discussion, in which Y being the charge balanced cations (Y=H^+, Li^+, Na^+, K^+) and M being the incorporated trivalent atoms (M=B, Al, Ga and Fe) and *x*MR the location of Y in the *x* (*x*=4,6,8) member ring. For example, the **H-Al-6MR** refers to the Al substituted SSZ-13-type zeolite, in which the proton located in the 6 MR is used to balance the charge.

3.1.1. Structures for Al substituted SSZ-13 zeolites. As shown in Fig. 2, the most stable structures for HAl-SSZ-13, LiAl-SSZ-13, NaAl-SSZ-13 and KAl-SSZ-13 zeolites are **H-Al-6MR**, **Li-Al-6MR**, **Na-Al-6MR** and **K-Al-8MR**, respectively. The results show that the most stable location for H, Li and Na is in the 6MR and tend to near the site of O4, while for K, the most stable location is in the 8MR near the site of O1. The main reason is that K is more diffuse and have much larger radius than H, Li and Na ,[56] the pore size of the 6MR is not large enough to host it, but the pore size of the 8MR does.[26]

For the HAl-SSZ-13, the site O4 is the best location for H (structure **H-Al-6MR)**, the proton also connected to the site O1 face to 8MR and 4MR with the relative energy 1 kJ • mol^{-1} and 21 kJ • mol^{-1} compared to Al-O4H-Si as show in Fig. S1. It is in good agreement with the reported experiments that the acidic O4H group is the only acid sites in the 6 MR, while O(1–3)H groups in the 8MR, with the lowest IR band at 3538 cm^{-1} among the 4 kinds of OH groups.[11] Although both of Li and Na have a similar location in the Al-SSZ-13 zeolites, the deformation of 6MR can be obviously observed for LiAl-SSZ-13. Further analysis for the bond distance, one can find that the distances for Li-O (in the range of 1.92~2.33 Å) are much shorter than these for Na-O (in the range of 2.29~2.47 Å). It indicates that Na is more favorable as a candidate than Li for the synthesizing of Al-SSZ-13 zeolites. It is confirmed that SSZ-13 is typically synthesized in the Na form and the other ions can be exchanged afterwards experimentally. These results are

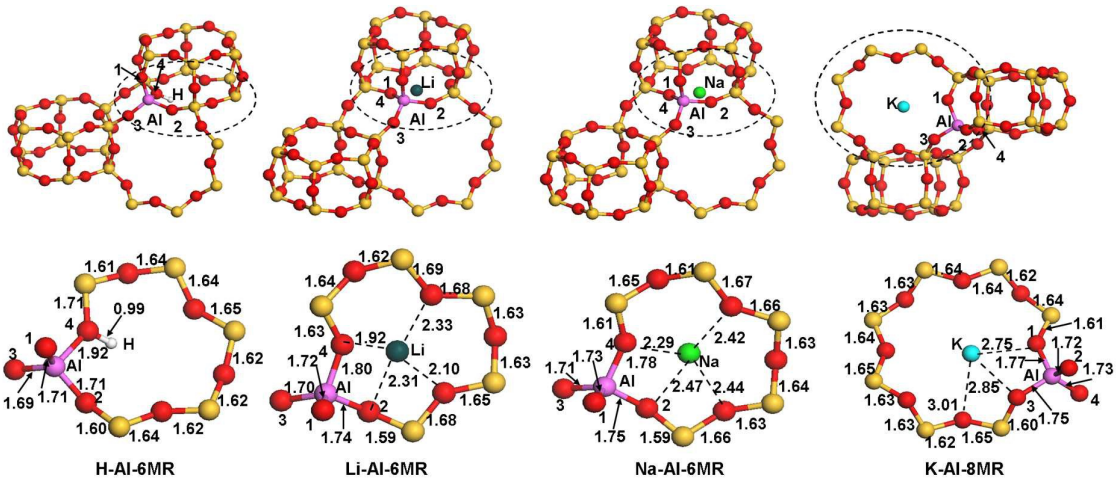

Fig. 2. The most stable structures for Al substituted SSZ-13-type zeolites. The H, Li, Na, K, O, Al and Si atoms are shown in white, dark slate green, green, blue, red, violet and yellow, respectively. The selective region is amplified to show the structural details. The selective distances are given in Å.

also in good agreement with the previous studies on NaAl-SSZ-13 zeolites.[57, 58]

Moreover, it is found that the bond distances from the Al to the O atom that near to the mono-valence ions are elongated to 1.92, 1.80 and 1.78 Å, which is in line with the previously calculated results in HAl-SSZ-13.[35] However, the distances for Si–O are in the range of 1.62~1.63 Å for HAl-SSZ-13, LiAl-SSZ-13 and NaAl-SSZ-13 as shown in Fig. 2, quite close to the experimental values of 1.60-1.62 Å for HAl-SSZ-13.[59] The distortion effect of Na to the framework of Al-SSZ-13 is less than H and Li, which indicates that radius size comparability (see Table S2 for radii) is essential for the charge-balanced ions. The size-matched charge-balanced ion such as Na is more stable than H and Li in the Al-SSZ-13 zeolites. These results are in line with our previously studied zeolites Al-MCM-22 and Al-MTW.[25, 60]

3.1.2. Structures for B substituted SSZ-13 zeolites. For B substituted SSZ-13 zeolites, the most stable structures are **H-B-6MR**, **Li-B-6MR**, **Na-B-8MR**, **K-B-8MR** for HB-SSZ-13, LiB-SSZ-13, NaB-SSZ-13 and KB-SSZ-13, respectively, which are slightly different from that of Al-SSZ-13 as show in Fig. 3. The most stable structure for NaB-SSZ-13 is located in 8MR as shown in structure **Na-B-8MR**, different from the NaAl-SSZ-13 in which

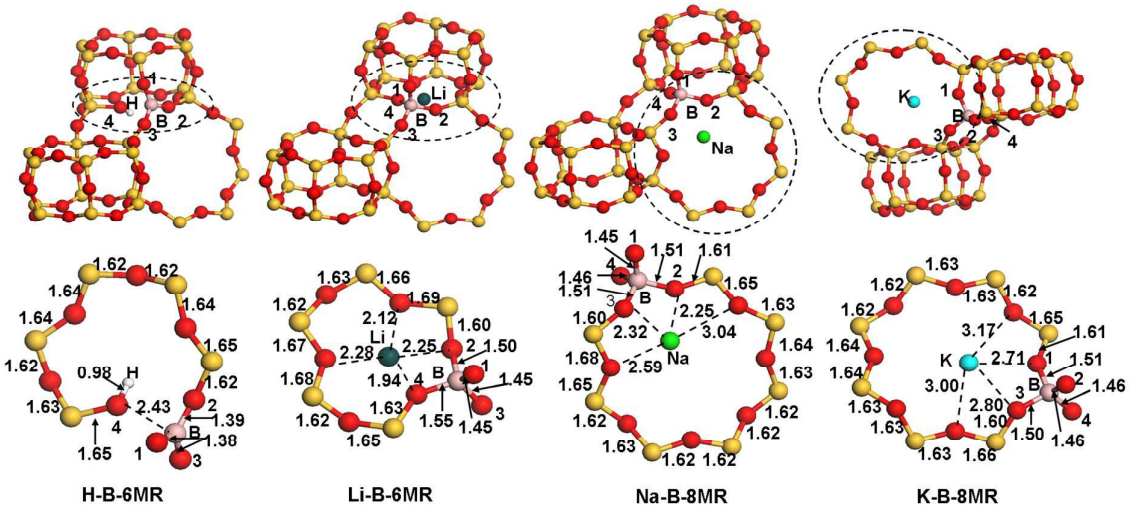

Fig. 3. The most stable structures for B substituted SSZ-13-type zeolites. The H, Li, Na, K, O, B, and Si atoms are shown in white, dark slate green, green, blue, red, tan and yellow, respectively. The selective region is amplified to show the structural details. The selective distances are given in Å.

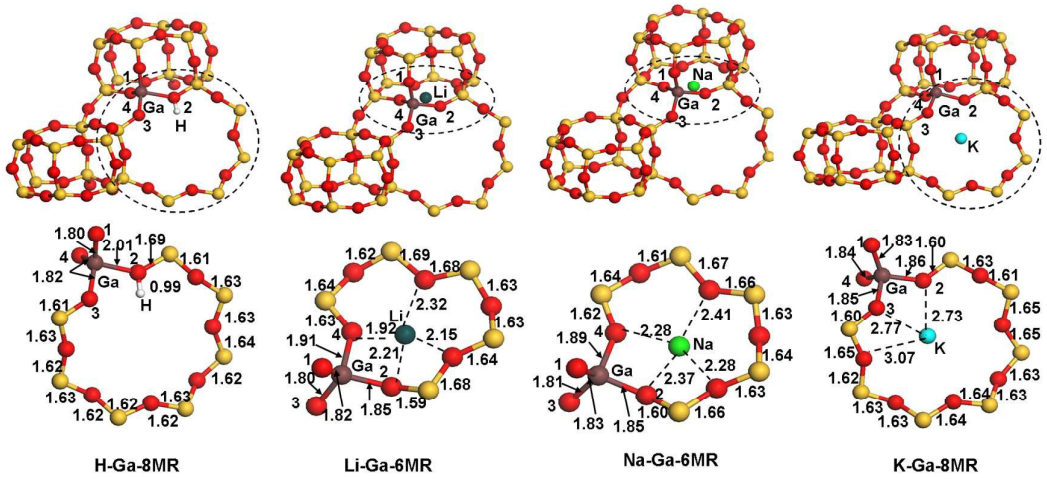

Fig. 4. The most stable structures for Ga substituted SSZ-13-type zeolites. The H, Li, Na, K, O, Ga and Si atoms are shown in white, dark slate green, green, blue, red, brown and yellow, respectively. The selective region is amplified to show the structural details. The selective distances are given in Å.

the Na is located in 6MR (**Na-Al-6MR** in Fig. 2). In addition, it is interesting to observe that B can not bond with the bridging -OH for the structure **H-B-6MR**. Instead, a closely resembling terminal silanol group is formed. The main reason is that the trigonal BO_3 is more stable than the tetrahedral BO_4 unit in B-incorporated zeolites.[39] These results are in good agreement with the DFT calculations on zeolites B-MCM-22 and B-MTW.[25, 60] Besides, the acid sites are also formed in the 8MR and 4MR, the relative energy are 1 and 33 kJ • mol^{-1} higher than that in the 6MR as show in Fig. S2. The most stable location for Li in the B-SSZ-13 is in 6 MR and near to the O4 with the shortest bond distance 1.94 Å. Clearly, it causes the deformation of 6 MR that the incorporation of mono-valent Li due to the radius difference between Na and Li, indicating that LiOH is not the best candidate for the synthesizing of SSZ-13 zeolites. It is also found that 8MR is a favor location for K in B-SSZ-13 similar to that for Al-SSZ-13. The nearest K-O distance is K-O1, which is shorted to 1.51 Å, similar to the B-O2 in the structure **Na-B-8MR**.

3.1.3. Structures for Ga substituted SSZ-13 zeolites. The most stable structures for HGa-SSZ-13, LiGa-SSZ-13, NaGa-SSZ-13 and KGa-SSZ-13 zeoliters are structure **H-Ga-8MR**, **Li-Ga-6MR**, **Na-Ga-6MR** and **K-Ga-8MR**, respectively (Fig. 4). It is interesting to note that the most favored location of proton is the 8MR for Ga-SSZ-13, different from Al-SSZ-13 and B-SSZ-13 zeolites. The main reason may lie in the larger radius of Ga, which significantly changes the structures of the framework of **H-Ga-8MR** as the distances are 1.80, 2.01, 1.82, 1.82 Å for Ga–

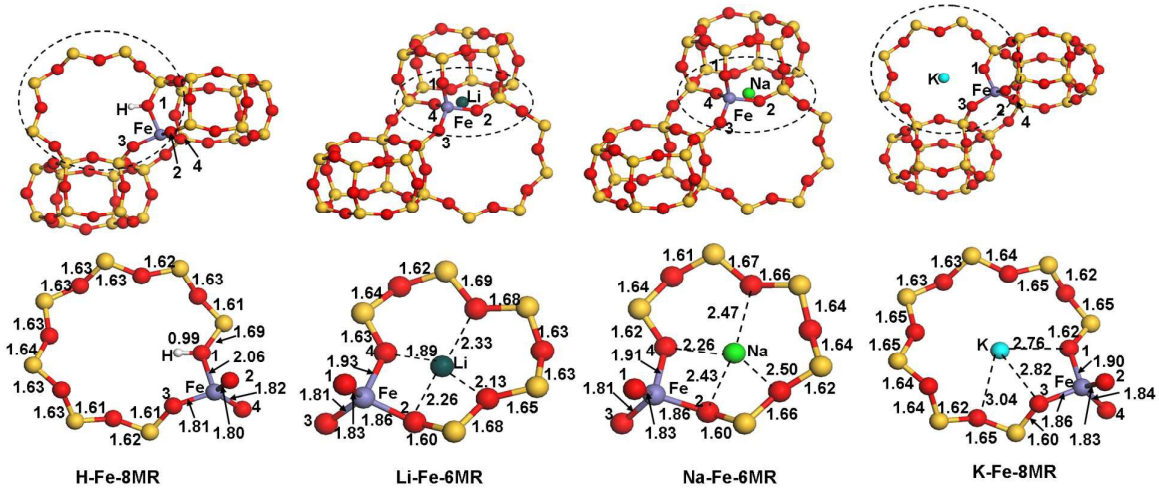

Fig. 5. The most stable structures for Fe substituted SSZ-13-type zeolites. The H, Li, Na, K, O, Fe and Si atoms are shown in white, dark slate green, green, blue, red, gray and yellow, respectively. The selective region is amplified to show the structural details. The selective distances are given in Å.

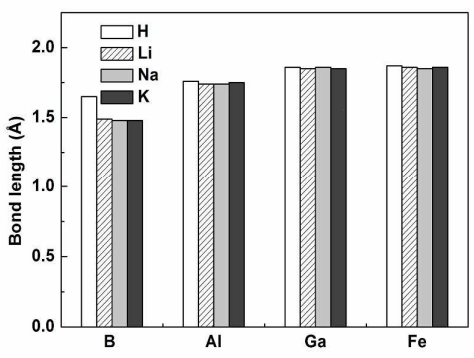

Fig 6. The average M–O (Å) bond distances for M substituted (M = B, Al, Ga and Fe) H-, Li-, Na- and K-form SSZ-13 zeolites.

O1, Ga–O2, Ga–O3, Ga–O4, respectively. They are systematically larger than that for Al-O, which is in the range of 1.71-1.92 Å. The structure change indicates that the incorporation of Ga in the framework of SSZ-13 is more difficult than Al, in agreement with the previous report on NCL-1 zeolites with the Si/M for Al, Ga and Fe incorporate NCL-1 zeolites in the same optimal synthetic condition is 83, 85 and 88, respectively.[61]

3.1.4. Structures for Fe substituted SSZ-13 zeolites. The most stable structures for HFe-SSZ-13, LiFe-SSZ-13, NaFe-SSZ-13 and KFe-SSZ-13 are structure **H-Fe-8MR**, **Li-Fe-6MR**, **Na-Fe-6MR** and **K-Fe-8MR**, respectively (Fig. 5). It is found that the position of charge balanced ions H+, Li+, Na+ and K+ are quite similar to that of Ga-SSZ-13 as the radius of Ga is quite near to that of Fe (see Table S2). The structure distortion also been observed for the 8MR of the structure **H-Fe-8MR**. The proton in the structure **H-Fe-8MR** is in the site O1 and the bond length Fe–O1 is elongated to 2.06 Å, which is longer than that of Al–O4 (1.92 Å, structure H-Al-6MR) and Ga–O2 (2.01 Å, structure H-Ga-8MR).

The most stable structures for B, Al, Ga and Fe substituted SSZ-13 with charge balanced by H^+, Li^+, Na^+ and K^+ show obvious different patterns. For the B, Al, Ga and Fe incorporated SSZ-13 zeolites, 6MR is always the most stable structure for Li-formed SSZ-13 and 8MR is always the most stable structure for K-formed SSZ-13 zeolites. The main reason is size comparability. The radius of K^+ is too larger to be hosted by neither the 6 MR nor the 4 MR, which was observed previously for MTW zeolites.[25] For the Li-form SSZ-13, the atom Li in the 6MR is more stable than that in the 8MR and 4MR. In addition, the incorporation of Li in the 6MR will significantly cause the distortion of 6MR compared to Na in the 6MR, which indicate that the Li is less stable than Na in the B, Al, Ga and Fe incorporated SSZ-13-type zeolites. It is found the most favored location for the H-form Al and B incorporated SSZ-13 zeolites is 6MR while the most favored location for the Ga and Fe incorporated SSZ-13 zeolites is 8MR.

However, comparing the most stable structures with the less stable structures, we found the energy differences is only 1~7 kJ • mol^{-1}. Such small energy difference indicates the location of proton (the Brønsted acid sites) can interchange even at room temperature. The Na tends to locate in 6MR, which was observed for Al, Ga and Fe incorporated zeolites. For the NaB-SSZ-13 zeolites, Na tends to locate in the 8MR. The main reason may attribute to the incorporation of B in the framework of SSZ-13 zeolites, which shortens the distance of B–O to 1.46~1.51 Å, leading to the 6MR too small to host the Na atom.

3.1.5. Geometric parameters. To study the relationship between the geometric parameters of SSZ-13-type zeolites and the substitutions of trivalent atoms (B, Al, Ga and Fe), Table S3 lists the volumes of the supercell and related bond distances. The H–O bond distances are 0.98, 0.99, 0.99 and 0.99 Å for H-form B, Al, Ga and Fe incorporated SSZ-13 zeolites, respectively, which are similar to the calculated H–O bonds in H_2O molecule (0.99 Å), H-form Al-MTW (0.99~1.03Å)[25] and H-form Al-BEA (0.98~1.00Å).[62] The distances from the proton and alkaline metal to its nearest O atom follow the order of H–O < NH4–O < Li–O < Na–O < K–O for the B, Al, Ga and Fe incorporated SSZ-13 zeolites.

The associated M–O (M=B, Al, Ga, Fe) bond distances and cell volumes of the zeolites increase with the increasing of atomic covalent radius of B, Al, Ga and Fe as shown in Fig. 6. The B–O bond distances of NH_4-B-SSZ-13, Li-B-SSZ-13, Na-B-SSZ-13, and K-B-SSZ-13 zeolites are in the range of 1.46~1.53, 1.45~1.55, 1.45~1.51, and 1.46~1.51 Å, respectively, leading to the tetra-coordinated B atoms. However, for the HB-SSZ-13, three B–O bond distances are 1.38~1.39 Å, while the other is 2.43 Å, which indicates that the B atom are three-fold coordinated for HB-SSZ-13. Similar cases were also found for Al, Ga and Fe incorporated H-form SSZ-13 zeolites. As show in Table S3 as well as Fig. 2–5, although Al, Ga and Fe are tetra-coordinated in H-Al-SSZ-13, H-Ga-SSZ-13, and H-Fe-SSZ-13 zeolites, one of the Al–O, Ga–O and Fe–O bonds are clearly elongated compared with the other three Al–O, Ga–O and Fe–O bonds, which may attribute to the weakening effect of associated H–O bonds.

To quantitatively evaluate the bond distance changes caused by the substitution atoms, the average bond distances of M–O are calculated and shown in Fig. 6. It was found that the average bond distances of M–O is in line with the radii of the substituted trivalent atoms by the order of B < Al < Ga $\approx$ Fe (see Table S2), which indicate the radii of the incorporation ions are essential for the structure deformation. The results show that the smaller radius differences of the incorporation ions to the Si atom are, the smaller changes of structure will be. The reason lies on the fact that the smaller difference of the incorporation ions to the Si atom will result in the smaller bond distance difference, subsequently leads to the smaller structure deformation.

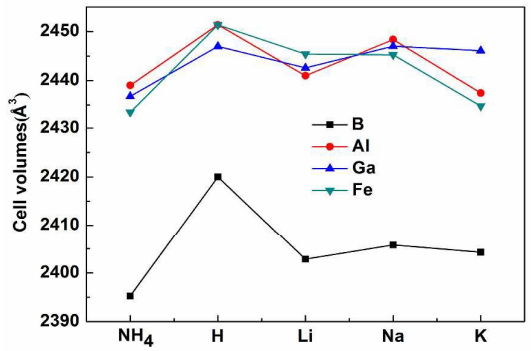

Fig 7. The cell volumes for the B, Al, Ga and Fe incorporated NH_4-, H-, Li-, Na- and K-form SSZ-13 zeolites.

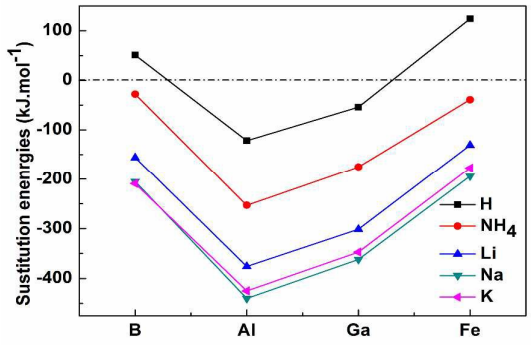

Fig. 8. Substitution energies for a Si atom substituted by a trivalent atom M (M = B, Al, Ga and Fe) for the H-, NH_4-, Li-, Na- and K-form SSZ-13-type zeolites.

The bond distance changes also lead to the significant change of the cell volumes. As shown in Fig. 7, it is found that the cell volumes of B-SSZ-13 zeolites are significantly smaller than the pure silica SSZ-13 and Al, Ga, and Fe substituted SSZ-13 zeolites due to the short B–O bond distances comparing to that of Si–O, Al–O, Fe–O and B–O bonds. It should be noted that one of the B–O distances for H-B-SSZ-13 is elongated to 2.43 Å, leading to the cell volume of the HB-SSZ-13 increased to 2420.00 Å^3, significantly larger than that of the Li- B-SSZ-13, NH_4- B-SSZ-13, Na- B-SSZ-13, and K- B-SSZ-13 zeolites.

3.2 Substitution energy

The calculated substitution energies are shown in Table S4 and tendency for the substitution energy are shown in Fig. 8. The results show that the substitution energies for Al, Ga and Fe incorporated SSZ-13 zeolites follow the order: H-form < NH_4-form < Li-form < K-form ≈ Na-form. It should be noted that the absolute value of substitution energies for Al-SSZ-13 are the largest, which indicates that the Al-incorporated SSZ-13 zeolites are more easily synthesized. In addition, it is interesting to indicate that the substitution energies for the H-form B-SSZ-13 and Fe-SSZ-13 zeolites are positive, which indicate that the synthesis of HB-SSZ-13 and HFe-SSZ-13 is thermodynamically unlikely. In contrast, the substitution energies for the NH_4-form B-SSZ-13 and Fe-SSZ-13 zeolites are a little more negative, which indicates that the synthesis of NH_4B- and NH_4Fe-SSZ-13 may be achieved, while the synthesis of NH_4B-SSZ-13 and NH_4Fe-SSZ-13 zeolites are considerably more difficult than that for Li-, Na- and K-form SSZ-13 zeolite. Moreover, it should be noted that the substitution energy for Na-form and K-form zeolites are quite close to each other, indicating Na and K are the suitable charge balanced ions for the synthesis of Al, Ga and Fe incorporate SSZ-13 zeolites.

3.3 Acid property

To evaluate the acidity of SSZ-13 zeolites, the adsorption of NH_3 and pyridine on both the Lewis and Brønsted acid sites were studied as NH_3 have successfully been used as the acidicity indication to measure the reactivity of a given site for CHA type zeolite AlPO-34 previously.[58] The adsorption energies for HB-SSZ-13, HAl-SSZ-13, HGa-SSZ-13 and HFe-SSZ-13 zeolites are listed in Table S5. The most stable structures, which have the largest adsorption energies for the adsorption of NH_3 on both Lewis and Brønsted acid sites in HB-SSZ-13, HAl-SSZ-13, HGa-SSZ-13 and HFe-SSZ-13 zeolites, are shown in Fig. 9. It is observed that the NH_3 can easily react with the proton of Brønsted acid sites to form NH_4^+ species except for HB-SSZ-13. As there is no NH_4^+ species for HB-SSZ-13, much weaker Brønsted acidity of HB-SSZ-13 zeolite is observed. The similar case is also observed for the adsorption of NH_3 adopted on the Lewis acid sites of H-SSZ-13 zeolites as the NH_3 could bond to the Lewis acid sites of HB-SSZ-13, HAl-SSZ-13, HGa-SSZ-13 and HFe-SSZ-13. After the adsorption of NH_3 on the Brønsted acid sites of the zeolites, the bond distances from the substituted atoms to the bridge oxygen atoms bonding with protons are enlarged obviously. For HAl-SSZ-13, HGa-SSZ-13, HFe-SSZ-13 and HB-SSZ-13 zeolites, the bond distances are 1.80, 1.87, 1.92 and 2.30 Å, respectively.

The most stable structures for the adsorption of pyridine on both Lewis and Brønsted acid sites in HB-SSZ-13, HAl-SSZ-13, HGa-SSZ-13 and HFe-SSZ-13 are shown in Fig. 10. It is observed that the pyridine can react with the proton of Brønsted acid sites to form $C_5NH_6^+$ for all the substituted SSZ-13. The distances from the H atom of $C_5NH_6^+$ to the nearest bridge oxygen atoms are 1.68, 1.66, 1.62 and 1.57 Å for the HB-SSZ-13, HAl-SSZ-13, HGa-SSZ-13 and HFe-SSZ-13, respectively. In comparison, the substituted atoms can also bond to pyridine to show the Lewis acidity except HB-SSZ-13 as HB-SSZ-13 exhibit the weakest Lewis acidity among these substituted zeolites as the distance from B to O atom of the OH group is elongated to 3.12 Å. However, the distances between the other substituted atoms and OH group are 2.19, 2.61 and 2.33 Å for HAl-SSZ-13, HGa-SSZ-13 and HFe-SSZ-13, respectively.

The adsorption energies tendency for the adsorption of NH_3 and pyridine are plotted in Fig. 11 to show the B, Al, Ga and Fe substitution effect for the NH_3 and pyridine adsorption on both the Lewis and Brønsted acid sites. From Fig. 11, we

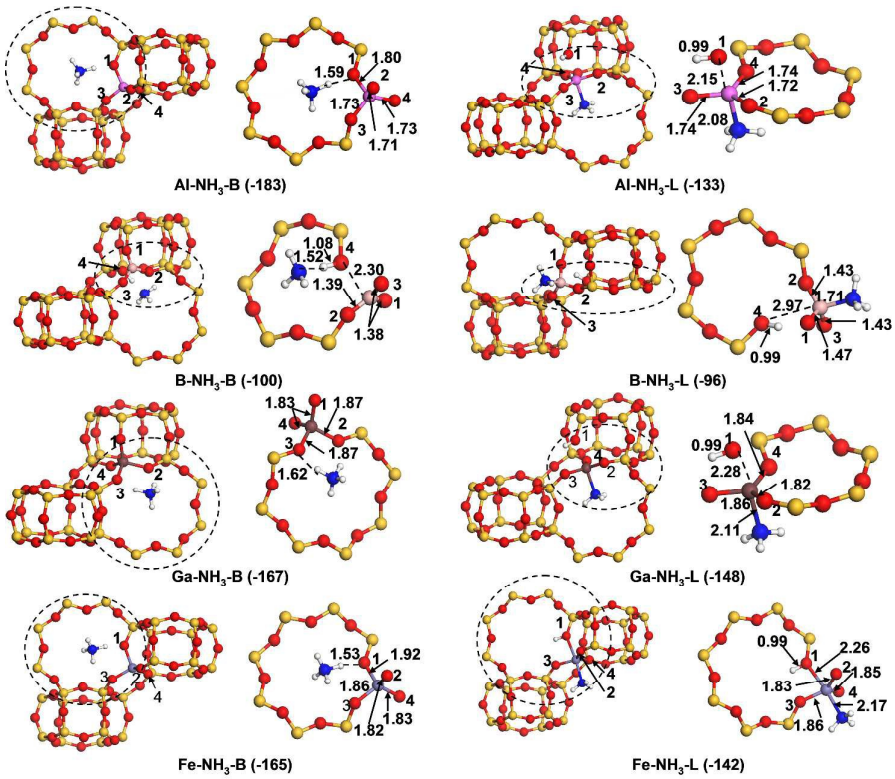

Fig. 9. The most stable structures for the adsorption of NH_3 inside B, Al, Ga and Fe incorporated H-form SSZ-13 zeolites. H, N, O, B, Al, Ga, Fe and Si atoms are shown in white, black blue, red, tan, violet, brown, gray and yellow, respectively. The selective region is amplified to show the structural details. A nomenclature is used as follows: B is the abbreviation for Brønsted acid site; L is the abbreviation for Lewis acid site. The adsorption energies are given in the parentheses.

can find that the adsorption energies for NH_3 are systematically smaller than that for pyridine on both Brønsted and Lewis acid sites. In addition, the adsorptions of NH_3 are found more favorable in the main channel (8 MRs) than in the cages (4 MRs), which is similar to the cases of NH_3 adsorption in the HAl-MTW[63] as the cages is too small to host the NH_3 molecules. As far as the substitution effect is concerned, we found that the Brønsted acid sites of the zeolites follow the order of HAl-SSZ-13 > HGa-SSZ-13 ≈ HFe-SSZ-13 > HB-SSZ-13 as the adsorption energies for HGa-SSZ-13 and HFe-SSZ-13 are close to each other. They are also in good agreement with the deprotonation energies (DPE in Table S7), which is another indication to measure the acidicity for various zeolites.[64-67] These results are also in line with that of the MCM-22 and MTW-type zeolites.[25, 60]

Comparing the adsorptions of NH_3 and pyridine on Brønsted acid sites with Lewis acid sites, we found the adsorption of NH_3 and pyridine on Brønsted acid sites is stronger than that on Lewis acid sites as the adsorption on the Lewis acid sites have to overcome the steric hindrance of Al-O bonds, which leads to different Lewis acidity order. From Fig. 11, the Lewis acidity of HB-SSZ-13 is found significant weaker than the others mainly due to the larger structural deformation. The adsorption energies show that the Lewis

Table 1. Brønsted acidicity order for the trivalent ions B, Al, Ga, Fe incorporated ZSM-5, MCM-22, MTW, CHA zeolites.

Type of Zeolites	Brønsted acidicity order	References
ZSM-5	B-ZSM-5<< Fe-ZSM-5 < Ga-ZSM-5 < Al-ZSM-5	68
MCM-22	B-MCM-22 < Fe-MCM-22 < Ga-MCM-22 < Al-MCM-22.	60
MTW	B-MTW < Fe-MTW≈Ga-MTW < Al-MTW	9, 25
CHA	B-SSZ-13 < Fe-SSZ-13≈Ga-SSZ-13< Al-SSZ-13	This work

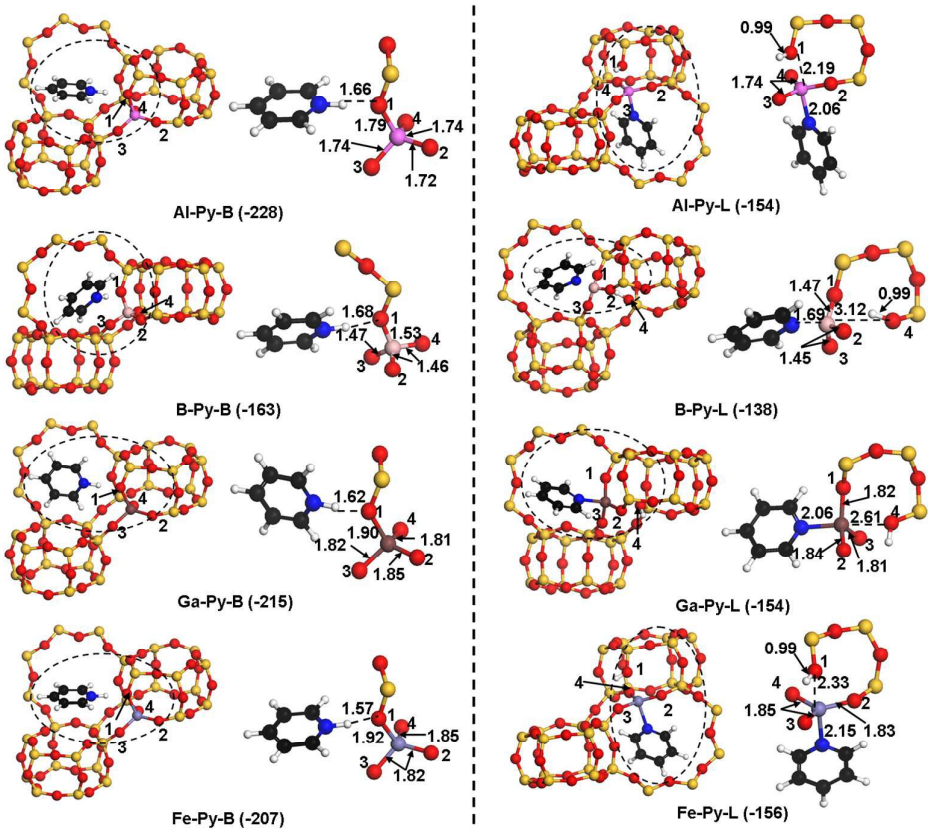

Fig. 10. The most stable structures for the adsorption of pyridine inside the B, Al, Ga and Fe incorporated H-form SSZ-13 zeolites. The selective region is amplified to show the structural details. The H, C, N, O, B, Al, Ga, Fe and Si atoms are shown in white, black, black blue, red, tan, violet, brown, gray and yellow, respectively. A nomenclature is used as follows: Py is the abbreviation for pyridine; B is the abbreviation for Brønsted acid site; L is the abbreviation for Lewis acid site.Brønsted acid site; L is the abbreviation for Lewis acid site. The adsorption energies are given in the parentheses.

acidity of HGa-SSZ-13 is similar to that of HFe-SSZ-13 for both the adsorption of NH_3 and pyridine, which leads to the acidity order as follows: HGa-SSZ-13 ≈ HFe-SSZ-13 > HAl-SSZ-13 > HB-SSZ-13.

We summarized the Brønsted acidicity order for the trivalent ions B, Al, Ga and Fe incorporated ZSM-5,[68] MCM-22,[60] MTW,[9, 25] and CHA zeolites as shown in Table 1. It was found that the acidity order for different type of zeolites are almost the same, i.e. the acidity of Brønsted sites is associated with the incorporation ions instead of the type of zeolites. Comparing the incorporation ions, we found that the larger radius differences of the incorporation ions to the Si atom are, the more acidity will be enhanced for the Brønsted sites. The reason lies on the fact that the larger difference of the incorporation ions to the Si atom will lead to the larger structure deformation and larger charge redistribution, subsequently lead to the Brønsted acidicity enhancement.

3.4 Bader charges analysis

To uncover the charge redistributions caused by the substitution, we studied those for B, Al, Ga and Fe substituted SSZ-13 zeolites and the detailed charge distributions are listed in Table S6. It is found that the charges of the alkali metals ions are +0.89, +0.86 and +0.92 for Li^+, Na^+ and K^+ in the B, Al, Ga and Fe substituted SSZ-13 zeolites unanimously. In addition, we observed that the charges of the substituted atoms distribution are independent of the charge balanced alkali ions. The charges are +2.39, +2.48, +1.77 and +1.45 for B, Al, Ga and Fe incorporated SSZ-13 zeolites, respectively, independent of the charge balanced alkali ions. However, the Brønsted acid site changes the charge distribution. For the B, Al, Ga and Fe incorporated H-form SSZ-13 zeolites, the charges of the substituted atoms are +2.36, +2.43, +1.75 and +1.43, respectively. They are obviously different from that of alkali balance B, Al, Ga and Fe incorporated SSZ-13 zeolites.

Fig. 12 shows the Bader charge distributions for the H of the Brønsted acid site, the associated bridged O, the trivalent atoms, the N in the pyridine and NH_3 adsorbed on the Lewis acid sites for the B, Al, Ga and Fe incorporated H-forms SSZ-13 zeolites. It is found that the charges of proton and bridge oxygens vary with the substituted atoms variation. The charge

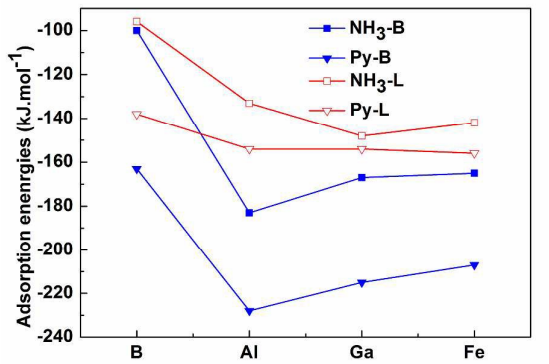

Fig. 11. Adsorption energies for the NH_3 and pyridine adsorption on the Brønsted and Lewis acid sites for the H-forms B, Al, Ga and Fe incorporated SSZ-13-type zeolites.

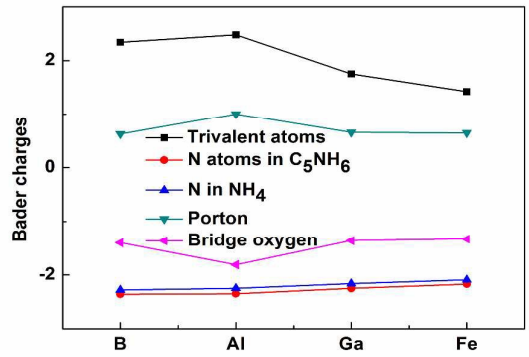

Fig. 12. Bader charge distributions for H, the associated bridged O, the trivalent atoms, the N in the pyridine and NH_3 adsorbed on the Lewis acid sites for the B, Al, Ga and Fe incorporated H-forms SSZ-13 zeolites.

for the protons are +0.62, +1.00, +0.65 and +0.64 for HB-, HAl-, HGa- and HFe-SSZ-13 zeolites, respectively. The charge on the Al atom is significantly larger than that of the other substituted atoms, confirming that the Al is indeed the most favorable substituted ion. Correspondingly, the charge is –1.81 for the bridged oxygen for HAl-SSZ-13, which is more negatively charged than that for HB-SSZ-13 (–1.40), HGa-SSZ-13 (–1.40) and HFe-SSZ-13 (–1.33).

For the adsorption of NH_3 and pyridine on the Lewis acid sites for the B, Al, Ga and Fe incorporated H-forms SSZ-13-type zeolites, the Bader charges are +2.34, +2.48, +1.75 and +1.42 for B, Al, Ga and Fe atoms, respectively, which indicating the B and Al atoms show trivalent properties whereas the Ga and Fe atom show divalent proporties. The reason may lie in the fact that the Ga and Fe have vacant *d* orbitals which may participate the bond formation whereas the B and Al do not have. Moreover, we found that the charge distributions on the N atoms of NH_3 and pyridine are almost the same from Fig. 12, which indicates the adsorption environments are similar. The Bader charge distributions shows the incorporation of Al is superior to the incorporation of B, Ga and Fe *et al.* trivalent ions due to size comparability.

Conclusions

The distribution schemes, the Brønsted and Lewis acidity properties of trivalent B, Al, Ga and Fe incorporated SSZ-13-type zeolites were comparatively studied by the dispersion-corrected density functional theory. It was found that the smaller radius differences of the incorporation ions, the smaller changes of the structures and the less enhancements of Brønsted acidity. The Al is found the most favorable trivalent incorporation ion among the studied trivalent ions and the Na^+ is found the most favorable charge balanced ion for the synthesis of SSZ-13-type zeolites due to the size comparability, which are in line with the experimental observation. Substitution studies shows that the incorporated trivalent ions B, Al, Ga and Fe in the H-, Li-, Na- and K-forms SSZ-13 zeolites are tetra-coordinated except HB-SSZ-13, in which three-fold coordination for B is favorable. Further studies on the locations for the charge balanced cations show that the K is favored to locate only in the main channel of the zeolites, while H, Li and Na can locate in both the 6MR and the main channel (8MR) of the zeolites. The cell volumes are found to be sensitive to charge balanced ions, in which the cell volumes of H-forms SSZ-13 zeolites are found lager than that of Li-, NH_4-, Na- and K-forms SSZ-13 zeolites. Substitution energy is introduced to evaluate SSZ-13-type zeolites relative synthesis difficulty for these incorporated zeolites with the following order: Al << Ga < B < Fe.

As indicated by the adsorption energies of NH_3 and pyridine in the zeolite, the adsorption of pyridine is significantly stronger than NH_3 adsorption. The Brønsted acid sites of the zeolites follow the order of HAl-SSZ-13 > HGa-SSZ-13 ≈ HFe-SSZ-13 > HB-SSZ-13. The Lewis acidity of HB-SSZ-13 is weaker than HAl-, HGa- and HFe-incorporated SSZ-13-type zeolites with the following order: HGa-SSZ-13 ≈ HFe-SSZ-13 > HAl-SSZ-13 > HB-SSZ-13. By the Bader charges analysis, the HAl-SSZ-13 is found the most strong Brønsted acid, while the Lewis acidity of HFe-SSZ-13 and HGa-SSZ-13 are almost the same and stronger than that of HAl-SSZ-13 and HB-SSZ-13. Our results provide new insights for synthesis for the SSZ-13-type zeolite and fundamental information for the zeolitic catalyst designation to enhance the catalytic performance.

Acknowledgements

This work was supported by the National Natural Science Foundation of China (20906067), CPSF (2011M500543), the Program for the Top Young Academic Leaders of Higher Learning Institutions of Shanxi and Research Project Supported by Shanxi Scholarship Council of China.

Notes and references

1 A. Corma, *Chem. Rev.*, 1997, **97**, 2373-2420.
2 C. S. Cundy and P. A. Cox, *Chem. Rev.*, 2003, **103**, 663-702.

3 F. Schwochow and L. Puppe, *Angew. Chem., Int. Ed. Engl.*, 1975, **14**, 620-628.
4 C. Martinez and A. Corma, *Coord. Chem. Rev.*, 2011, **255**, 1558-1580.
5 S. I. Zones, *J. Chem. Soc., Faraday Trans.*, 1991, **87**, 3709-3716.
6 S. I. Zones and R. A. Van Nordstrand, *Zeolites*, 1988, **8**, 166-174.
7 B. Liu, Y. Zheng, N. Hu, T. Gui, Y. Li, F. Zhang, R. Zhou, X. Chen and H. Kita, *Micropor. Mesopor. Mater.*, 2014, **196**, 270-276.
8 L. S. Dent and J. V. Smith, *Nature*, 1958, **181**, 1794-1796.
9 G. Feng, Z.-H. Lu, D. Yang, D. Kong and J. Liu, *Micropor. Mesopor. Mater.*, 2014, **199**, 83-92.
10 M.-J. Diaz-Cabanas and P. A. Barrett, *Chem. Commun. (Camb.)*, 1998, 1881-1882.
11 K. Suzuki, G. Sastre, N. Katada and M. Niwa, *Phys. Chem. Chem. Phys.*, 2007, **9**, 5980-5987.
12 R. Shah, J. D. Gale and M. C. Payne, *Chem. Commun. (Camb.)*, 1997, 131-132.
13 Q. Zhu, J. N. Kondo, T. Tatsumi, S. Inagaki, R. Ohnuma, Y. Kubota, Y. Shimodaira, H. Kobayashi and K. Domen, *J. Phys. Chem. C*, 2007, **111**, 5409-5415.
14 T. Inui and M. Kang, *Appl. Catal., A*, 1997, **164**, 211-223.
15 Y. Hasegawa, C. Abe, F. Mizukami, Y. Kowata and T. Hanaoka, *J. Membr. Sci.*, 2012, **415**, 368-374.
16 U. Deka, A. Juhin, E. A. Eilertsen, H. Emerich, M. A. Green, S. T. Korhonen, B. M. Weckhuysen and A. M. Beale, *J. Phys. Chem. C*, 2012, **116**, 4809-4818.
17 H. Kalipcilar, T. C. Bowen, R. D. Noble and J. L. Falconer, *Chem. Mater.*, 2002, **14**, 3458-3464.
18 M. R. Hudson, W. L. Queen, J. A. Mason, D. W. Fickel, R. F. Lobo and C. M. Brown, *J. Am. Chem. Soc.*, 2012, **134**, 1970-1973.
19 Q. Zhu, M. Hinode, T. Yokoi, J. N. Kondo, Y. Kubota and T. Tatsumi, *Micropor. Mesopor. Mater.*, 2008, **116**, 253-257.
20 F. Gao, M. Kollar, R. K. Kukkadapu, N. M. Washton, Y. Wang, J. Szanyi and C. H. F. Peden, *Appl. Catal., B*, 2015, **164**, 407-419.
21 F. Goltl, R. E. Bulo, J. Hafner and P. Sautet, *J. Phys. Chem. Lett.*, 2013, **4**, 2244-2249.
22 F. Goltl, P. Sautet and I. Hermans, *Angew. Chem., Int. Ed. Engl.*, 2015, **54**, 7799-7804.
23 M. Zokaie, U. Olsbye, K. P. Lillerud and O. Swang, *Micropor. Mesopor. Mater.*, 2012, **158**, 175-179.
24 S. Yuan, J. Wang, Y. Li and S. Peng, *J. Mol. Catal. A: Chem.*, 2001, **175**, 131-138.
25 G. Feng, D. Yang, D. Kong, J. Liu and Z.-H. Lu, *RSC adv.*, 2014, **4**, 47906-47920.
26 R. Nedyalkova, C. Montreuil, C. Lambert and L. Olsson, *Top. Catal.*, 2013, **56**, 550-557.
27 G. Košová and J. Čejka, *Collect. Czech. Chem. Commun.*, 2002, **67**, 1760-1778.
28 S. Namuangruk, P. Pantu and J. Limtrakul, *J. Catal.*, 2004, **225**, 523-530.
29 H. C. Xin, X. P. Li, Y. Fang, X. F. Yi, W. H. Hu, Y. Y. Chu, F. Zhang, A. M. Zheng, H. P. Zhang and X. B. Li, *J. Catal.*, 2014, **312**, 204-215.
30 A. Zheng, H. Zhang, L. Chen, Y. Yue, C. Ye and F. Deng, *J. Phys. Chem. B*, 2007, **111**, 3085-3089.
31 G. Yang, L. J. Zhou and X. W. Han, *J. Mol. Catal. A: Chem.*, 2012, **363**, 371-379.
32 A. M. Zheng, L. Chen, J. Yang, M. J. Zhang, Y. C. Su, Y. Yue, C. H. Ye and F. Deng, *J. Phys. Chem. B*, 2005, **109**, 24273-24279.
33 G. Yang, E. A. Pidko and E. J. M. Hensen, *J. Phys. Chem. C*, 2013, **117**, 3976-3986.
34 D. E. Akporiaye, I. M. Dahl, H. B. Mostad and R. Wendelbo, *J. Phys. Chem.*, 1996, **100**, 4148-4153.
35 Y. Jeanvoine, J. G. Angyan, G. Kresse and J. Hafner, *J. Phys. Chem. B*, 1998, **102**, 5573-5580.
36 A. H. de Vries, P. Sherwood, S. J. Collins, A. M. Rigby, M. Rigutto and G. J. Kramer, *J. Phys. Chem. B*, 1999, **103**, 6133-6141.
37 X. Solans-Monfort, M. Sodupe, V. Branchadell, J. Sauer, R. Orlando and P. Ugliengo, *J. Phys. Chem. B*, 2005, **109**, 3539-3545.
38 J. Liang, J. Su, Y. Wang, Z. Lin, W. Mu, H. Zheng, R. Zou, F. Liao and J. Lin, *Micropor. Mesopor. Mater.*, 2014, **194**, 97-105.
39 L. Regli, C. Lamberti, C. Busco, A. Zecchina, C. Prestipino, K. P. Lillerud, S. I. Zones and S. Bordiga, *From Zeolites to Porous Mof Materials: The 40th Anniversary of International Zeolite Conference, Proceedings of the 15th International Zeolite Conference*, 2007, **170**, 585-593.
40 L. Regli, S. Bordiga, C. Busco, C. Prestipino, P. Ugliengo, A. Zecchina and C. Lamberti, *J. Am. Chem. Soc.*, 2007, **129**, 12131-12140.
41 R. Fricke, H. Kosslick, G. Lischke and M. Richter, *Chem. Rev.*, 2000, **100**, 2303-2406.
42 M. Kang and C.-T. Lee, *J. Mol. Catal. A: Chem.*, 1999, **150**, 213-222.
43 P. P. Knops-Gerrits and W. A. Goddard, *J. Mol. Catal. A: Chem.*, 2001, **166**, 135-145.
44 L.-T. Yuen, S. I. Zones, T. V. Harris, E. J. Gallegos and A. Auroux, *Micropor. Mater.*, 1994, **2**, 105-117.
45 G. Kresse and J. Furthmüller, *Comp. Mater. Sci.* , 1996, **6**, 15-50.
46 G. Kresse and J. Furthmüller, *Phys. Rev. B*, 1996, **54**, 11169-11186.
47 S. Grimme, *J. Comput. Chem.*, 2006, **27**, 1787-1799.
48 T. Kerber, M. Sierka and J. Sauer, *J. Comput. Chem.*, 2008, **29**, 2088-2097.
49 J. W. Liu, Z. F. Liu, G. Feng and D. J. Kong, *J. Phys. Chem. C*, 2014, **118**, 18496-18504.
50 J. W. Liu, F. Mohamed and J. Sauer, *J. Catal.*, 2014, **317**, 75-82.
51 J. P. Perdew, K. Burke and M. Ernzerhof, *Phys. Rev. Lett.*, 1996, **77**, 3865-3868.
52 P. E. Blochl, C. J. Forst and J. Schimpl, *Bull. Mater. Sci.*, 2003, **26**, 33-41.
53 P. E. Blöchl, *Phys. Rev. B*, 1994, **50**, 17953-17979.
54 N. J. Mosey, P. Liao and E. A. Carter, *J. Chem. Phys.*, 2008, **129**, 014103.
55 A. B. Munoz-Garcia, D. E. Bugaris, M. Pavone, J. P. Hodges, A. Huq, F. L. Chen, H. C. zur Loye and E. A. Carter, *J. Am. Chem. Soc.*, 2012, **134**, 6826-6833.
56 J. K. Park, *J. Phys. Chem. A*, 2002, **106**, 3008-3016.
57 F. Goltl and J. Hafner, *J. Chem. Phys.*, 2011, **134**, 064102.
58 C. M. Wang, R. Y. Brogaard, B. M. Weckhuysen, J. K. Norskov and F. Studt, *J. Phys. Chem. Lett.*, 2014, **5**, 1516-1521.

59 L. J. Smith, A. Davidson and A. K. Cheetham, *Catal. Lett.*, 1997, **49**, 143-146.
60 Y. Wang, D. Zhou, G. Yang, S. Miao, X. Liu and X. Bao, *J. Phys. Chem. A*, 2004, **108**, 6730-6734.
61 M. Sasidharan, S. G. Hegde and R. Kumar, *Micropor. Mesopor. Mater.*, 1998, **24**, 59-67.
62 T. Demuth, J. Hafner, L. Benco and H. Toulhoat, *J. Phys. Chem. B*, 2000, **104**, 4593-4607.
63 G. Feng, Y.-Y. Lian, D. Yang, J. Liu and D. Kong, *Can. J. Chem.*, 2013, **91**, 925-934.
64 G. Yang, X. Liu, X. Han and X. Bao, *J. Phys. Chem. B*, 2006, **110**, 23388-23394.
65 A. Zheng, H. Zhang, X. Lu, S.-B. Liu and F. Deng, *J. Phys. Chem. B*, 2008, **112**, 4496-4505.
66 H. Fang, A. Zheng, S. Li, J. Xu, L. Chen and F. Deng, *J. Phys. Chem. C*, 2010, **114**, 10254-10264.
67 N. Feng, A. Zheng, S.-J. Huang, H. Zhang, N. Yu, C.-Y. Yang, S.-B. Liu and F. Deng, *J. Phys. Chem. C*, 2010, **114**, 15464-15472.
68 C. T. W. Chu and C. D. Chang, *J. Phys. Chem.*, 1985, **89**, 1569-1571.
69

